Constraining oxygen consumption by nitrite oxidation in oceanic oxygen minimum zones

Beman, J.M.[1], S.M. Vargas[1], J.M. Wilson[1,2], E. Perez-Coronel[1], S. Vazquez[1], A. Yu[1], A.E. Cairo[1], J.S. Karolewski[3], S.D. Wankel[3]

[1]Life and Environmental Sciences, University of California, Merced, Merced, CA, USA
[2]Scripps Institution of Oceanography, University of California, San Diego, CA, USA
[3]Marine Chemistry and Geochemistry, Woods Hole Oceanographic Institution, Woods Hole, MA, USA

Corresponding author: Prof. J. Michael Beman, Life and Environmental Sciences, University of California, Merced, 5200 North Lake Road, Merced, CA 95343, USA
E-mail: jmbeman@gmail.com
Phone: +1.650.823.7925

Author Contributions
J.M.B. designed the study and performed the research with S.M.V, J.M.W., E.P.C., S.V., A.Y., A.C., and J.S.K.; S.D.W. contributed new analytical tools, and J.M.B. wrote the paper.

Competing Interest Statement: The authors have no competing interests.

This PDF file includes:
Main Text
Figures 1 to 5
Tables 1 to 2

Main Text Word Count: 5,282
Reference Count: 54

Abstract

Oceanic oxygen minimum zones (OMZs) occur where microorganisms deplete dissolved oxygen (DO) to exceptionally low levels, and are globally significant sites of biogeochemical cycling. Amid the intense competition for DO and other substrates occurring in these metabolically challenging environments, aerobic nitrite oxidation may consume significant amounts of DO, but this has not been examined comprehensively. Using parallel measurements of oxygen consumption rates and ^{15}N-nitrite oxidation rates applied to water column profiles and to oxygen manipulation experiments, we show that nitrite oxidation is a substantial sink for DO in the ocean's largest OMZ. The contribution of nitrite oxidation to overall DO consumption increased at low DO concentrations, tracking gradients and variations within and across multiple stations in the eastern tropical North Pacific Ocean. Oxygen manipulation experiments produced highly consistent effects, with nitrite oxidation responsible for progressively more DO consumption (up to 97%) as DO was experimentally decreased. Natural abundance stable isotope data indicated coupling of nitrite oxidation and nitrate reduction, while 16S rRNA and metagenome sequencing revealed that *Nitrospina* ecotypes possessing high-affinity cytochrome oxidase genes were prevalent and active within the OMZ. Collectively, our results demonstrate that nitrite oxidation consumes significant amounts of DO, and that this proportion increases as DO declines—indicating that nitrite oxidation is critically important to the formation and maintenance of OMZs.

Significance

Oceanic oxygen minimum zones (OMZs) are naturally-occuring regions of low oxygen found in select areas of the ocean. Lack of dissolved oxygen has important implications for both the distribution of marine organisms and global biogeochemical cycles, yet we have a limited understanding of how oxygen is depleted to such low levels. Here we comprehensively quantify the contribution of nitrite oxidation to oxygen depletion in the ocean's largest OMZ. We observed highly consistent patterns across depth profiles, and in multiple experiments where we manipulated oxygen concentrations, finding that nitrite oxidation consumes progressively more oxygen at lower oxygen concentrations. Our findings demonstrate that nitrite oxidation plays a pivotal role in exhausting oxygen to the low levels found in OMZs.

Introduction

Aerobic nitrite oxidation is pervasive throughout much of the oceanic water column, playing a central role in deep ocean chemoautotrophy and carbon cycling (1, 2), as well as in the oceanic nitrogen (N) cycle (3, 4). Nitrite oxidation rates are typically undetectable using $^{15}NO_2^-$ isotopic tracer in the sunlit euphotic zone, peak at the base of the euphotic zone, and subsequently decline with depth (5). However, nitrite oxidation rate profiles deviate from this pattern in oceanic oxygen minimum zones (OMZs) that are depleted in dissolved oxygen (DO): rapid rates have been reported despite low DO concentrations (6–9), and nitrite oxidation itself may consume DO to low levels. OMZs are ultimately generated by high sinking fluxes of organic matter combined with reduced ventilation at depth, and are typically defined by DO concentrations <20 μM (10). Regions of the tropical oceans containing no measurable DO—termed anoxic marine zones (AMZs; ref. 11)—are further distinguished by the accumulation of nitrite to comparatively high (>1 μM) concentrations (12). These secondary nitrite maxima (SNM) result from anaerobic nitrate reduction to nitrite under low DO (11–13). Accumulated nitrite may be subsequently reduced via denitrification and anaerobic ammonium oxidation (14)—or, alternatively, oxidized by NOB. Nitrite is therefore rapidly produced and consumed via multiple processes in OMZs, linking the oceans' N, carbon, and oxygen cycles.

Despite its centrality in OMZ biogeochemical cycles, nitrite oxidation is still poorly understood in these regions of the ocean. In particular, high rates of nitrite oxidation where DO levels are intrinsically low indicates that marine nitrite-oxidizing bacteria (NOB) may contribute substantially to DO depletion and the ultimate generation and maintenance of OMZs. However, this contribution to O_2 drawdown has not been directly quantified. While nitrite oxidation has been measured in several OMZs (6–9), oxygen consumption rate (OCR) measurements in OMZs are rare (15). Yet simultaneous measurements are necessary to directly quantify the contribution of nitrite oxidation to oxygen consumption.

An additional distinguishing feature of AMZs is the presence of a deep chlorophyll maximum (DCM) where distinct ecotypes of the globally important cyanobacterium, *Prochlorococcus*, produce DO within low DO waters (16–18). DCM-based DO production can overlap with nitrite supply via nitrate reduction, but the degree to which nitrite oxidation (versus other processes) consumes DO in the DCM remains poorly constrained (18).

90 Our understanding of how NOB oxidize nitrite under low O_2 is also evolving. NOB gain
91 energy by oxidizing nitrite to nitrate while using dissolved oxygen (DO) as a terminal electron
92 acceptor. Adaptations to low DO are evident in different NOB, and both *Nitrospina* and
93 *Nitrococcus* may contribute to varying degrees (19, 20). But although *in situ* nitrite oxidation
94 rates are typically highest under low DO, experimental oxygen manipulations show the opposite
95 pattern: declining rates with declining DO (21). This may be explained by variations in genomic
96 content among different NOB that allow them to occupy distinct, highly-resolved DO niches
97 throughout the water column (4, 7, 21)—including those that occur from the edge (20 μM) to the
98 core (<5 nM) of OMZs. These details are essential to understand in the context of ocean
99 deoxygenation, as seemingly small variations in DO may have significant biogeochemical
100 implications if different ecotypes within different functional groups—such as nitrite oxidizers,
101 nitrate reducers, and organisms respiring organic matter aerobically—have varying sensitivities
102 to DO.
103 Here we address these open questions through parallel measurements of nitrite oxidation
104 and overall OCR in the oceans' largest OMZ, the eastern tropical North Pacific Ocean (ETNP).
105 Nitrite oxidation rate measurements (using $^{15}NO_2^-$), OCR measurements (using optical sensor
106 spots), and ammonia oxidation rate measurements (using $^{15}NH_4^+$) were made along depth
107 profiles at six stations in the ETNP, including three OMZ stations and three AMZ stations
108 (Figure 1). At each station, we sampled in the upper 100 m to capture the primary nitrite
109 maximum and an expected peak in nitrite oxidation rates at the base of the euphotic zone (EZ).
110 We then sampled a range of DO values (from 200 μM to the anoxic SNM at AMZ stations) to
111 quantify rate variations in response to vertical gradients in DO. How nitrite oxidation varies
112 from the OMZ edge to its anoxic core is critical to our understanding of ocean biogeochemical
113 cycles; we therefore conducted oxygen manipulation experiments and examined the response of
114 nitrite oxidation and OCR. Combined with natural abundance stable isotope data, 16S rRNA
115 sequences, and metagenomes, we show that nitrite oxidation is a substantial, and occasionally
116 even dominant, sink for oxygen in the ETNP.
117
118 **Results and Discussion**
119 *Nitrite oxidation rates in the ETNP*

We sampled six stations in the ETNP OMZ with low (<20 μM) DO concentrations at depth (Figs 1 and 2). Three stations extending out from the coast of Mexico (Stations 1-3) were AMZ stations with distinct DCMs and accumulations of nitrite in SNMs indicative of anaerobic N cycling (Figure 2A and B). We expected that these would be hotspots of nitrite oxidation given oxygen supply via photosynthesis in the DCM overlapping with nitrite supply via nitrate reduction. Across all stations and depths, we observed the highest nitrite oxidation rates at the AMZ stations (Fig. 2C). Station 1 is located nearest the coast and had a shallow OMZ at the time of our sampling, with 20 μM DO at 28 m depth, and nitrite > 1 μM at 100 m. Chlorophyll concentrations were also high in the upper water column (up to 5 mg m^{-3} at 20 m), with a DCM spanning 75-125 m. Nitrite oxidation displayed a local maximum at the base of the EZ at Station 1 (20-30 m), and then increased to higher levels (>100 nmol L^{-1} d^{-1}). This increase at 100 m corresponded with the overlap between the bottom of the DCM and the top of the SNM. Nitrite oxidation rates then reached higher values at 125 and 150 m within the SNM at Station 1. Stations 2 and 3 displayed similar nitrite oxidation rate profiles to each other, including elevated rates in the DCM and SNM. Nitrite oxidation rates were similar in magnitude, and peak values at the base of the EZ and in the OMZ were also similar (69-96 nmol L^{-1} d^{-1}). Depth patterns tracked oceanographic differences across the three AMZ stations, as the depth of all features increased moving offshore from Station 1 to 2 to 3 (Fig. 2). For example, the DCM extended from 105-155 m at Station 2, while nitrite concentrations began to increase below 100 m; nitrite oxidation rates were elevated at 140 m and declined slightly with increasing depth. At Station 3, the DCM (120-180 m) and SNM (>140 m) depths were deeper, and nitrite oxidation rates increased from 100 to 200 m.

In contrast to these three AMZ stations (Stations 1-3), rate profiles at Stations 4-6 showed peaks at the base of the EZ and decreases with depth, with no subsurface increase within the OMZ (*SI Appendix,* Figure S1). Parallel measurements of ammonia oxidation rates also showed this type of pattern at all stations (*SI Appendix*, Fig. S1). Subsurface maxima in ammonia oxidation tracked variations in the EZ across all six stations, but rates were not elevated in OMZ/AMZ waters—again contrasting with nitrite oxidation rate profiles at the AMZ stations. These data accord with earlier work in OMZs showing contrasting ammonia and nitrite oxidation rate profiles, and particularly high rates of nitrite oxidation in OMZ waters (6–8, 22-24). Elevated nitrite oxidation below the DCM (> 120 m at Station 1, >155 m at Station 2, and >180

151 m at Station 3), where little to no DO is available, could have a number of possible explanations
152 discussed below. Within the DCM, our data support the idea that nitrite oxidation contributes to
153 'cryptic' oxygen cycling (18)—i.e., that DO produced via oxygenic photosynthesis is rapidly
154 consumed.
155
156 *Oxygen consumption via nitrite oxidation*
157 We determined the contribution of nitrite oxidation to overall oxygen consumption via parallel
158 measurements of oxygen consumption rates (OCR) using *in situ* optical sensor spots—which are
159 non-invasive, compare favorably with other low-level measurement approaches, are the only
160 cost-effective means of achieving of substantial replication, and for which sensitivity increases
161 under low DO (25, 26). Decreases in DO were measured in both nitrite and ammonia oxidation
162 rate sample bottles, as well as in three additional replicates, to leverage statistical power for
163 increased sensitivity to low-level DO consumption (see Materials and Methods). Water column
164 OCR profiles at all stations showed exponential declines with depth and decreasing DO
165 concentrations (Fig. 2D and S1). OCR magnitudes were similar to the limited previous
166 measurements that have been conducted in OMZs (e.g., 161-2600 nmol L^{-1} d^{-1} in ref 15). OCR
167 also tracked variations in DO across stations, with progressively steeper declines in OCR with
168 depth from Station 6 through Station 1. This pattern of declining OCR with increasing depth and
169 decreasing DO contrasted with that of nitrite oxidation rates, which were notably elevated under
170 low DO (Fig. 2).
171 OCR was not significantly different from zero at >125 m at Station 1 and >140 m at
172 Stations 2 and 3, obviously owing to the initial lack of DO at these depths at the AMZ stations.
173 However, typically 1-2 out of 5 replicates did contain DO introduced during sampling and
174 incubation. Short of conducting *in situ* incubations, such DO contamination is essentially
175 unavoidable. However, all microorganisms and metabolic processes exposed to DO may
176 capitalize on its introduction and directly compete for DO. We directly compared nitrite
177 oxidation rates with OCR, assuming that each mole of nitrite is oxidized using ½ mole of O_2 (5).
178 (As the O added to nitrite to form nitrate comes from water, and ^{15}N is used to measure the rate,
179 it is possible that oxidants other than DO are used; see below.) We found that nitrite oxidation
180 increased as a proportion of overall OCR at lower DO levels (Figure 3A and B). Nitrite
181 oxidation was responsible for up to 69% of OCR at Station 1, although most values were closer

182 to 10-40% at Stations 2 and 3 (Fig. 3). In contrast, ammonia oxidation contributed no more than
183 5% in the OMZ (*SI Appendix*, Fig. S1).
184
185 *Effects of oxygen manipulation experiments on nitrite oxidation and OCR*
186 These data indicate that NOB are poised to rapidly consume any DO introduced to sample
187 bottles, although they may be partly affected by sample collection and manipulation. We
188 therefore verified these observations by experimentally manipulating DO concentrations to
189 measure the response of OCR, as well as $^{15}NO_2^-$ nitrite oxidation rates, to changing DO (Figure
190 4). We conducted experiments on the edge of the OMZ (depth of 20 μM DO) at Stations 1-5, in
191 the DCM at Stations 2 and 3, and in the SNM at Station 3 and an additional sampling Station 3.5
192 (Table 1). (We could not conduct additional experiments at Stations 1 and 2 owing to a
193 hurricane in the region at the time of sampling in 2018, and added Station 3.5 as a result.)
194 Oxygen manipulations were designed to quantify nitrite oxidation and OCR across the spectrum
195 of DO concentrations that occur from the OMZ edge to its core—rather than solely probing their
196 lower limits—in order to constrain rate responses to changing DO within OMZs.
197 Oxygen manipulation experiments were consistent with water column profiles and
198 provide additional evidence that nitrite oxidation can be a substantial oxygen sink. In all
199 experiments, we found that OCR declined with experimentally decreased DO (Fig. 4). All
200 curves displayed Michaelis-Menten type forms; however, we note that mixed assemblages of
201 microorganisms drive this overall pattern by using DO to oxidize a variety of substrates. These
202 substrates can include nitrite, as well as different forms of organic matter, reduced sulfur
203 compounds, and possibly methane (27). Consistent with earlier work (21), nitrite oxidation rates
204 also displayed Michaelis-Menten-type curves in most of our experiments (Fig. 4). However,
205 nitrite oxidation rates were less sensitive to declining DO than OCR. Nitrite oxidation was
206 therefore responsible for progressively higher proportion of overall OCR as DO was
207 experimentally decreased (Fig. 3C). In fact, we found that 97% of OCR in the DCM at Station 2
208 could be explained by measured nitrite oxidation rates, while most values were closer to 10-20%.
209 This pattern in experiments was notably similar to results from rate profiles (Fig. 3B and C).
210 Based on these data, we calculated the DO level at which nitrite oxidation may be
211 expected to consume all DO. As the data above indicate, this is obviously variable across
212 experiments: our experiment in the DCM at Station 2 showed that nitrite oxidation can consume

213 essentially all available DO (Fig. 4 C), while the experiment with 20 μM [DO] water at Station 2
214 suggests that, even at low DO levels, nitrite oxidation would not consume all DO (Fig. 4B). We
215 fit Michaelis-Menten-type curves to nitrite oxidation rates and OCR individually (Table 1;
216 although these are, again, mixed microbial assemblages). Calculated DO affinities (K_s values)
217 were substantially lower for nitrite oxidation compared with OCR, particularly in the DCM
218 (Stations 2 and 3) and SNM (Stations 3 and 3.5). Based on these relationships, OCR always
219 exceeds nitrite oxidation on the OMZ edge, but nitrite oxidation is estimated to consume all DO
220 below concentrations of 35-96 nM in the SNM and DCM.
221 These data tie together multiple aspects of OMZ biogeochemistry into a coherent picture.
222 Although nitrite oxidation rates decline as DO is experimentally decreased at individual depths—
223 and so with particular assemblages of NOB—different depths/assemblages display different
224 properties (Fig. 4). More importantly, this decline is always less severe for nitrite oxidation than
225 for overall OCR (Figs. 2-4). NOB are therefore highly effective at scavenging low levels of DO
226 (Figs. 3 and 4; (18), which is consistent with the idea of a nitrogen-oxygen feedback loop in
227 OMZs driven partly by oxygen depletion via nitrite oxidation (28).
228
229 *Isotopic, 16S rRNA, and metagenomic constraints on nitrite oxidation*
230 To further verify our findings, we applied natural abundance stable isotope measurements, 16S
231 rRNA sequencing, and metagenome sequencing to water samples and nucleic acid samples
232 collected in parallel with nitrite oxidation rate measurements (Figure 5). The dual N and O
233 isotopic composition of dissolved nitrate ($\delta^{15}N$ and $\delta^{18}O$, respectively; *SI Appendix* Fig. S2) is
234 thought to provide an effective constraint on nitrite oxidation under low DO conditions due to
235 isotopic 'overprinting' by nitrite oxidation (29, 30). While the respiratory reduction of nitrate
236 (denitrification) leads to equal 1:1 increases in $\delta^{15}N$ and $\delta^{18}O$ (31, 32), deviations in 1:1 N:O
237 isotope behavior arise from a decoupling of the N and O systems. These deviations are widely
238 interpreted as reflecting cryptic re-oxidation of nitrite under low DO, where the reduction of
239 nitrate to nitrite removes an O atom, and the subsequent re-oxidation of nitrite to nitrate appends
240 a new O atom derived from ambient water (33, 34). Deviations from the 1:1 relationship are
241 represented via $\Delta(15,18)$ values (35), where more negative values represent larger departures
242 from the 1:1 relationship.

At Stations 1-3, dual nitrate isotope values exhibited non-linear trends (Figure 5B and *SI Appendix* Fig. S3) that are consistent with isotopic overprinting by nitrite oxidation (29, 30). Δ(15,18) values were lowest (i.e., deviations were largest) at 50-150 m at Station 1, 100-140 m at Station 2, and 110-160 m at Station 3. The lower portions of these depth ranges overlapped with the upper portion of the DCM (75-125 m, 105-155 m, and 120-180 m, respectively) and tracked depth variations between stations. Peak deviations at Stations 1 and 2 were just above the DCM (75 and 100 m), while the peak at Station 3 corresponded closely with the DCM (140 m). Throughout these ETNP OMZ sites, our nitrate isotope data are consistent with previous observations and interpretations of rapid recycling between nitrate and nitrite (29, 35, 36), ultimately evidenced by isotopic overprinting of the nitrate reduction signal by nitrite oxidation.

16S rRNA gene and transcript sequencing revealed a similar pattern to rate profiles, experiments, and isotopic data, while also enabling identification of NOB that are abundant and active in the ETNP OMZ. Based on DNA, *Nitrospina* 16S rRNA amplicon sequence variants (ASVs; ref. 37) comprised up to 3.4-5.4% of all ASVs at Stations 1-3 (Fig. 5C), and relative abundances were strikingly consistent with the isotopic anomalies—abundances and anomalies were well-correlated (r^2=0.70-0.84, $P<0.05$) at Stations 1 and 3, for instance. These patterns were accentuated for RNA samples, but with discrete peaks in 16S rRNA transcripts generally occurring at deeper depths (Fig. 5D). *Nitrospina* 16S rRNA peaked at 125 m at Sta 1 (1.8% of all 16S rRNA transcripts; with an additional upper water column peak at 50 m), 140 m at Station 2 (3.2%), and particularly 140-180 m at Station 3 (1.6-7.1%). All of these depths lie within the DCM at each station. Although 20 *Nitrospina* ASVs were identified, three were dominant (each >1% of all ASVs, together constituting 72-100% of all *Nitrospina* 16S rRNA gene sequences and transcripts). One of these ASVs was found only in OMZ samples at Stations 1-3, and was not detected above the OMZ or at Stations 4 and 5. This was also the lone ASV observed in the OMZ at Station 3, where *Nitrospina* were most active based on their comparatively high percentages of all 16S rRNA transcripts. In contrast, no *Nitrococcus* ASVs and only one low-abundance *Nitrospira* ASV were identified out of >11,000 ASVs and >3.5 million 16S sequences from 73 DNA and 73 RNA samples. In line with earlier work in the ETNP (7, 19), other OMZs (6, 38), and the varaitions in DO affinity observed across oxygen manipualtion experiments (Fig. 4), these results indicate that particular *Nitrospina* ecotypes—and one ASV in

273 particular—are significant for low-oxygen nitrite oxidation, while other ASVs may be more
274 important at different depths and DO concentrations.
275 To validate the genetic potential for nitrite oxidation by *Nitrospina* under low DO
276 concentrations, we sequenced metagenomes collected on the OMZ edge, at the DCM, and within
277 the OMZ core at Stations 1, 2, and 3. Nitrite oxidoreductase genes from *Nitrospina* were
278 prevalent at all stations and depths, establishing the genomic potential for nitrite oxidation
279 throughout the ETNP OMZ (Table 2). In addition, multiple high-affinity cytochrome C oxidase
280 genes from *Nitrospina* were present in all samples—indicating that *Nitrospina* are capable of
281 consuming DO at the low concentrations found within the OMZ. These genes were more
282 common in DCM and SNM metagenomes than at the OMZ edge, consistent with *Nitrospina*
283 ecotype distributions, and with the lower DO concentrations found at the DCM and SNM.
284 Cytochrome *bd*-type oxidase genes from *Nitrospina* were also detected in all metagenomes
285 except the OMZ edge sample at Station 1, although these lack quinol binding sites and may not
286 functional as canonical oxidases (19, 39). Sun et al. (19) also suggested that chlorite dismutase
287 genes may be relevant for anaerobic metabolism in *Nitrospina*, and these were present in all
288 metagenomes. Finally, *Prochlorococcus* genes were prevalent from the OMZ edge to core, and
289 especially within the DCM, supporting the idea that oxygenic photosynthesis and cryptic oxygen
290 cycling occur throughout the ETNP OMZ. Overall, metagenomic data are consistent with
291 experimental data and 16S data, and indicate *Nitrospina* are tightly tuned to DO concetrations in
292 the ETNP.
293
294 *Oxygen consumption by nitrite oxidation in OMZs*
295 Assembled together, our results provide a comprehensive view of nitrite oxidation and its
296 contribution to oxygen consumption in the ocean's largest OMZ. Rate measurements, oxygen
297 manipulation experiments, stable isotopic data, and molecular data all converge on the fact that
298 nitrite oxidation is active from the base of the euphotic zone into the OMZ. Nitrite oxidation was
299 particularly significant within the DCM at Stations 1-3: nitrite oxidation rates were elevated,
300 isotopic overprinting of nitrate by nitrite oxidation was evident, and *Nitrospina* were abundant
301 and active (Fig. 2C and 5). All of these data tracked consistent progression in the depth of the
302 DCM across stations, and indicate that nitrite oxidation is important is important for DO
303 utilization in the DCM. Based on rate profiles, nitrite oxidation ranged from 10-47% of OCR in

the DCM, while experiments indicate maximum percentages of 13-97% (Fig. 3B and 3C). Stations 4-6—which lack a DCM and SNM—provide a notable contrast, as do ammonia oxidation rate profiles (Fig. S1).

Peaks in the magnitude of departure from a 1:1 nitrate reduction signal (e.g., isotopic overprinting by nitrite oxidation), and in *Nitrospina* ASV abundances, further indicate that nitrite oxidation is active above and below the DCM (Fig. 5). At Stations 2 and 3, nitrite oxidation rates above the DCM were similar to rates deeper in the water column. Station 1, in contrast, showed a rate increase within the AMZ. While rate measurements may reflect consumption of introduced DO, *Nitrospina* 16S rRNA transcripts increased in relative abundance within the AMZ. RNA samples were collected from the CTD rosette and rapidly filtered, so if these data capture a response to oxygen exposure, this response is exceptionally rapid and consistent. Alternatively, these data indicate that *Nitrospina* are active within the AMZ. One possibility is that *Nitrospina* survive anaerobically for periods of time until provided DO (40). Alternative oxygen-evolving mechanisms from nitrite have also been proposed for anaerobic methane-oxidizing bacteria (41) that are active in OMZs (42). Finally, the presence of *Prochlorococcus* below the DCM may allow low-level DO production via oxygenic photosynthesis (Table 2). Regardless of the mechanism, isotopic data and 16S rRNA data are consistent with transient nitrite oxidation coupled to nitrate reduction below the DCM.

However, our primary focus was on oxygen consumption via nitrite oxidation and its implications for the formation, maintenance, and expansion of OMZs. Two clear and consistent patterns emerged from both water column profiles and oxygen manipulation experiments: (i) overall OCR declined with decreasing DO in profiles and experiments, while (ii) nitrite oxidation increased as a proportion of OCR as DO declined in both profiles and experiments (Fig. 3B and 3C and 4). Variation in the proportion of OCR explained by nitrite oxidation from depth to depth and experiment to experiment was superimposed on these two patterns. Nitrite oxidation was significant throughout the OMZ and experiments—typically ranging from 10-40% of OCR—and sometimes dominant. For example, nitrite oxidation responded rapidly to introduced DO in the SNM at Station 1, and evidently consumed all DO produced in the DCM at Station 2.

Variation in the proportion of overall OCR attributable to nitrite oxidation could reflect fluctuations through time (28), as well as differences in substrate availabilities and affinities relative to DO for different processes consuming DO. Other than nitrite oxidation, aerobic

335 respiration of organic matter is probably most significant for OCR given relative substrate
336 concentrations (organic C > CH_4 or reduced S compounds; refs. 42–44), as well as high affinities
337 for DO among heterotrophic bacteria (45–47). Notably, many aerobic heterotrophs are also
338 facultatively anaerobic, switching to nitrate reduction under low DO (13, 48). Along with a
339 general decline in aerobic respiration rates with decreasing DO, this switch to nitrate reduction
340 may explain the steep declines in OCR that we observed in our experimental data. Production of
341 nitrite from nitrate reduction may also jumpstart nitrite oxidation, and is consistent with isotopic
342 data. We suggest that such cryptic nitrite/nitrate cycling may explain the adaptations of
343 particular *Nitrospina* ASVs to AMZs: although these are low-DO environments, they are also
344 high-nitrite environments, representing a trade-off in the availability of electron donor and
345 acceptor. The costs of life at low DO may be offset by the advantages of consistently elevated
346 nitrite concentrations.

347 In line with this idea, we found that the proportion of DO consumed by nitrite oxidation
348 increased at progressively lower DO concentrations in both profiles and experiments (Fig. 3B
349 and C). This consistent pattern demonstrates that nitrite oxidation increases in relative
350 importance as DO declines, and suggests that nitrite oxidation may play a critical role in the shift
351 from low oxygen (an OMZ) to functional anoxia (an AMZ). Moreover, our results indicate that
352 nitrite oxidation is carried out by just a few *Nitrospina* ASVs—in contrast with the diversity of
353 other microbial groups that may be involved in overall oxygen consumption (4, 49). Put another
354 way, even when nitrite oxidation represents a relatively modest proportion of OCR, just one to
355 three ASVs may be responsible for this contribution to overall oxygen consumption. *Nitrospina*
356 are therefore instrumental in DO consumption, and disproportionately important as DO declines.
357 When coupled to nitrate reduction, this could result in an oxygen consumption feedback loop
358 fueled by cryptic nitrite/nitrate cycling. Rate profiles, oxygen manipulation experiments, natural
359 abundance measurements, 16S rRNA sequencing, and metagenomic data all favor this idea: as
360 DO declines, OCR decreases precipitously while nitrite oxidation does not; the low-oxygen
361 adaptations of particular *Nitrospina* support high abundances and activity; and isotopic
362 anomalies are consistent with strong coupling between nitrite oxidation and nitrate reduction.
363 Our data convincingly establish that nitrite oxidation is pivotal in oxygen and nitrogen cycling in
364 OMZs, and so central in the creation and maintenance of these biogeochemically-important
365 regions of the ocean.

366

367 **Materials and Methods**

368 **Sample Collection.** Samples were collected in April 2017 and June 2018 aboard the *R/V*
369 *Oceanus*. At each station, conductivity/salinity, temperature, depth, pressure, chlorophyll
370 fluorescence, and photosynthetically active radiation (PAR) were measured by a SeaBird SBE-
371 9plus CTD, SBE-3F temperature sensor, SBE-43 DO sensor, WetLabs ECO-FLR Fluorometer,
372 and Biospherical QCP2200 PAR sensor. Initial casts were used to measure DO and nutrient
373 profiles to guide subsequent sampling. Nutrient samples were analyzed for NH_4^+ and NO_2^-
374 aboard the ship, with additional shore-based analyses of combined NO_3^-+NO_2^- and PO_4^{3-} at the
375 University of California Santa Barbara Marine Science Institute Analytical Lab (*SI Appendix,*
376 *Supplementary Materials and Methods*).

377 At all stations, water samples were collected in the upper 100 m to capture variation in
378 the upper water column, and we then sampled across a range of DO levels and nitrite levels to
379 capture variation in the OMZ. Samples were collected at 200, 100, 50, 20, 10, 5, and 1 μM [DO]
380 at all stations. Because the OMZ is shallower and more intense moving south and nearshore in
381 the ETNP (Fig. 1), these DO levels can occur within the upper 100 m, such that upper 100 m and
382 DO-based sampling overlapped. This overlap was greater at Station 1, followed by 2 and 3. At
383 these AMZ stations, samples were also collected at three depths between the 1 μM [DO] level
384 and the SNM.

385

386 **OCR Measurements and Oxygen Manipulations**. Two types of sensor spots were used to
387 measure OCR and manipulate DO, one with a wider range and detection limit of 100 nM (Fibox,
388 Loligo Systems, Viborg, Denmark), as well as trace-level spots with a detection limit of 10 nM
389 (FireSting, Pyroscience, Aachen, Germany) (26). Loligo sensor spots were used for water
390 column profiles given the wider DO range, while FireSting trace-level spots were used to
391 establish deoxygenation experiments and measure OCR within them. Optical sensors were
392 calibrated using DO-saturated water and sodium sulfite-saturated and He-purged water. On the
393 upper end, Fibox sensor spot DO measurements were highly correlated with CTD DO values
394 (r^2=0.996, slope=0.997) for [DO] > 1 μM. On the lower end, we regularly checked the '0 nM'
395 concentration with repeated measurements of sodium sulfite-saturated water and He-purged
396 water, and our lowest values measured in experiments were consistently within 5 nM of 0. In

397 both profiles and experiments, OCR was measured as the linear decrease in DO over the course
398 of experiments (25, 50). Experiments were conducted for 24 hours in the dark in a cold van
399 adjusted to ambient temperature, with separate incubations (and therefore temperatures)
400 conducted for samples from the upper 100 m, for oxygen/nitrite-based sampling, and for
401 deoxygenation experiments at each station.
402 Water column profiles of OCR were measured using 5 replicates at each depth, including
403 one each with tracer level (5-10% *in situ* concentration measured at sea) addition of $^{15}NH_4^+$ or
404 $^{15}NO_2^-$ to measure ammonia/nitrite oxidation (see below). Loligo sensor spots were attached to
405 the inside of 300 mL Wheaton BOD glass bottles using silicone glue prior to the cruise. At sea,
406 bottles were filled to at least three times overflowing via slow laminar flow, were rapidly capped
407 and transferred to the cold van, and initial DO measurements were made. After incubation,
408 endpoint DO measurements were made and then 50 mL samples from relevant bottles were
409 frozen for nitrite and ammonia oxidation rate measurements.
410 Oxygen manipulation experiments were conducted in 500 mL serum bottles with
411 attached FireSting sensor spots. For each experiment, a total of 24 bottles were filled with water
412 collected at a specific depth, sealed, and then bubbled with ultrapure He gas while DO was
413 monitored. 8 bottles had tracer-level $^{15}NO_2^-$ additions, 8 bottles had tracer-level $^{15}NH_4^+$
414 additions, and 8 were unlabeled. In each set of 8 bottles, we established initial DO values
415 typically ranging from 10s to 1000s of nM (Figure 4). OCR was measured in all bottles based on
416 starting and ending DO values, and samples for nitrite oxidation were collected from $^{15}NO_2^-$
417 labeled bottles at the end of the experiments. For all experiments, dedicated bottles were used
418 for the different ^{15}N labels.
419
420 **Nitrate isotopic measurements.** Both natural abundance and ^{15}N-tracer-based nitrate isotopes
421 were quantified by use of the denitrifier method (51, 52), in which 20-30 nmoles of NO_3^- were
422 quantitatively converted to N_2O by a culture of the denitrifying bacterium, *Pseudomonas*
423 *aureofaciens*. Product N_2O was cryogenically purified and trapped under flow of ultra-high
424 purity He, before being introduced to an IsoPrime 100 isotope ratio mass spectrometer. Isotope
425 ratios were normalized to international reference materials (USGS 32, USGS 34, USGS 35) and
426 reported using standard delta notation. Any nitrite present in the sample was removed by
427 addition of sulfamic acid (31). In samples from the upper 100 m, where NO_3^- concentrations

428 were low, 'carrier' NO_3^- of known isotopic composition was added and sample compositions
429 were calculated by mass balance. Precision of natural abundance isotope ratio measurements
430 was ±0.3‰ and ±0.4‰ for $\delta^{15}N$ and $\delta^{18}O$, respectively. $\delta^{15}N$ and $\delta^{18}O$ values were used to
431 calculate the Δ(15,18) deviation from the 1:1 line following Sigman et al. (35).
432
433 **Nitrite Oxidation Rates.** Nitrite oxidation rates were measured by adding 98 atom percent
434 (atom%) $^{15}NO_2^-$ to a final concentration of 12-184 nmol L^{-1}—representing 5-10% of *in situ* NO_2^-
435 concentrations (with the exception of some samples in the upper 100m with no measurable
436 nitrite)—and measuring the accumulation of ^{15}N label in the NO_3^- pool following Beman et al.
437 (7). After incubation for ~24 hours, samples were frozen at sea. Upon thawing in the laboratory,
438 excess $^{15}NO_2^-$ was removed following Granger and Sigman (31). In brief, sulfamic acid (~8-10
439 μL mL^{-1}) was added, the samples were shaken and allowed to sit for >5 minutes, and then
440 samples were neutralized by adding NaOH (4 M, ~11 μL mL^{-1}) prior to analysis.
441 Rates of $^{15}NO_2^-$ oxidation ($^{15}R_{ox}$) were calculated using equation 1 from Beman et al. (7)
442 adapted from Ward et al. (53):

443 $$^{15}R_{ox} = \frac{\left(n_t - n_{oNO_3^-}\right) \times \left[NO_3^-\right]}{\left(n_{NO_2^-}\right) \times t} \quad (1)$$

444 where n_t is the atom% ^{15}N in NO_3^- measured at time t, $n_{oNO_3^-}$, is the measured atom% ^{15}N of
445 unlabeled NO_3^-, $[NO_3^-]$ is the concentration of the NO_3^- pool, and $n_{NO_2^-}$ is the exponential
446 average atom% of NO_2^- over time t. $n_{NO_2^-}$ was calculated by isotope mass balance based on
447 initial NO_2^- concentrations, measured isotopic composition, added ^{15}N-labeled NO_2^-, and
448 measured $^{15}NH_4^+$ oxidation rates (which produce unlabeled NO_2^-; ammonia oxidation rate
449 measurements followed Beman et al. (23)).
450
451 **RNA/DNA Extractions, 16S rRNA Sequencing and Analysis, and Metagenome Sequencing**
452 **and Analysis** are reported in the *SI Appendix, Supplementary Materials and Methods.*
453
454 **Sequence data** are available in the Sequence Read Archive under BioProjects PRJNA192803
455 (16S data), and PRJNA634212 (metagenomes).
456

Statistical analyses were carried out in the R statistical environment (RStudio Version 1.0.136). Linear regressions were performed using the 'lm' function in R; Michaelis-Menten curve fits were performed using the 'drm' function in the R package drc (54).

Acknowledgments

This work was supported by NSF CAREER grant OCE-1555375 to J.M.B. Metagenome sequencing was supported by the UCMEXUS-CONACyT Collaborative Grants Program (to J.M.B. and José García Maldonado). We thank the officers and crew of the *R/V Oceanus* for their help at sea, and thank Sarah Abboud, Daniela Alonso, DeVonyo Bills, Jorge Montiel Molina, and Kevin Testo for their assistance in the field.

References

1. M. G. Pachiadaki, *et al.*, Major role of nitrite-oxidizing bacteria in dark ocean carbon fixation. *Science* **358**, 1046–1051 (2017).
2. M. A. Saito, *et al.*, Abundant nitrite-oxidizing metalloenzymes in the mesopelagic zone of the tropical Pacific Ocean. *Nat. Geosci.* **13**, 355–362 (2020).
3. C. A. Francis, J. M. Beman, M. M. M. Kuypers, New processes and players in the nitrogen cycle: The microbial ecology of anaerobic and archaeal ammonia oxidation. *ISME J.* **1**, 19–27 (2007).
4. A. D. Bertagnolli, F. J. Stewart, Microbial niches in marine oxygen minimum zones. *Nat. Rev. Microbiol.* **16**, 723–729 (2018).
5. B.B. Ward, "Nitrification in Marine Systems" in Nitrogen in the Marine Environment, 2nd Ed., D. Capone, D. Bronk, M. R. Mulholland, E. Carpenter, Eds. (Elsevier Inc., 2008), pp. 199-263.
6. J. Füssel, *et al.*, Nitrite oxidation in the Namibian oxygen minimum zone. *ISME J.* **6**, 1200–1209 (2012).
7. J. M. Beman, J. Leilei Shih, B. N. Popp, Nitrite oxidation in the upper water column and oxygen minimum zone of the eastern tropical North Pacific Ocean. *ISME J.* **7**, 2192-2205 (2013) https:/doi.org/10.1038/ismej.2013.96.
8. X. Peng, *et al.*, Ammonia and nitrite oxidation in the Eastern Tropical North Pacific. *Global Biogeochem. Cycles* **29**, 2034–2049 (2015).

9. X. Sun, Q. Ji, A. Jayakumar, and B.B Ward, Dependence of nitrite oxidation on nitrite and oxygen in low-oxygen seawater. *Geophysical Res. Lett.* **44**, 7883-7891 (2017).
10. A. Paulmier, D. Ruiz-Pino, Oxygen minimum zones (OMZs) in the modern ocean. *Prog. Oceanogr.* **80**, 113–128 (2009).
11. O. Ulloa, D. E. Canfield, E. F. DeLong, R. M. Letelier, F. J. Stewart, Microbial oceanography of anoxic oxygen minimum zones. *Proc. Natl. Acad. Sci. U. S. A.* **109**, 15996–16003 (2012).
12. B. Thamdrup, T. Dalsgaard, N. P. Revsbech, Widespread functional anoxia in the oxygen minimum zone of the Eastern South Pacific. *Deep. Res. Part I Oceanogr. Res. Pap.* **65**, 36–45 (2012).
13. D. Tsementzi, *et al.*, SAR11 bacteria linked to ocean anoxia and nitrogen loss. *Nature* **536**, 179–183 (2016).
14. A. R. Babbin, R. G. Keil, A. H. Devol, B. B. Ward, Organic matter stoichiometry, flux, and oxygen control nitrogen loss in the ocean. *Science* **344**, 406–408 (2014).
15. T. Kalvelage, *et al.*, Aerobic Microbial Respiration In Oceanic Oxygen Minimum Zones. *PLoS One* **10**, e0133526 (2015).
16. R. Goericke, R. J. Olson, A. Shalapyonok, A novel niche for Prochlorococcus sp. in low-light suboxic environments in the Arabian Sea and the Eastern Tropical North Pacific. *Deep. Res. Part I Oceanogr. Res. Pap.* **47**, 1183–1205 (2000).
17. P. Lavin, B. González, J. F. Santibáñez, D. J. Scanlan, O. Ulloa, Novel lineages of Prochlorococcus thrive within the oxygen minimum zone of the eastern tropical South Pacific. *Environ. Microbiol. Rep.* **2**, 728–738 (2010).
18. E. Garcia-Robledo, *et al.*, Cryptic oxygen cycling in anoxic marine zones. *Proc. Natl. Acad. Sci. U. S. A.* **114**, 8319–8324 (2017).
19. X. Sun, *et al.*, Uncultured Nitrospina-like species are major nitrite oxidizing bacteria in oxygen minimum zones. *ISME J.* **13**, 2391–2402 (2019).
20. J. Füssel, *et al.*, Adaptability as the key to success for the ubiquitous marine nitrite oxidizer Nitrococcus. *Sci. Adv.* **3**, e1700807 (2017).
21. L. A. Bristow, *et al.*, Ammonium and nitrite oxidation at nanomolar oxygen concentrations in oxygen minimum zone waters. *Proc. Natl. Acad. Sci. U. S. A.* **113**, 10601–10606 (2016).

22. P. Lam, *et al.*, Revising the nitrogen cycle in the Peruvian oxygen minimum zone. *Proc. Natl. Acad. Sci. U. S. A.* **106**, 4752-7 (2009).
23. J. M. Beman, B. N. Popp, S. E. Alford, Quantification of ammonia oxidation rates and ammonia-oxidizing archaea and bacteria at high resolution in the Gulf of California and eastern tropical North Pacific Ocean. *Limnol. Oceanogr.* **57**, 711–726 (2012).
24. F. Lipschultz, *et al.*, Bacterial transformations of inorganic nitrogen in the oxygen-deficient waters of the Eastern Tropical South Pacific Ocean. *Deep Sea Res. Part A, Oceanogr. Res. Pap.* **37**, 1513–1541 (1990).
25. M. Holtappels, *et al.*, Aquatic respiration rate measurements at low oxygen concentrations. *PLoS One* **9** (2014).
26. P. Lehner, *et al.*, LUMOS - A sensitive and reliable optode system for measuring dissolved oxygen in the nanomolar range. *PLoS One* **10**, 1–15 (2015).
27. W. F. Gilly, J. M. Beman, S. Y. Litvin, B. H. Robison, Oceanographic and Biological Effects of Shoaling of the Oxygen Minimum Zone. *Ann. Rev. Mar. Sci.* **5**, 393–420 (2013).
28. J. L. Penn, T. Weber, B. X. Chang, C. Deutsch, Microbial ecosystem dynamics drive fluctuating nitrogen loss in marine anoxic zones. *Proc. Natl. Acad. Sci. U. S. A.* **116**, 7220–7225 (2019).
29. J. Granger, S. D. Wankel, Isotopic overprinting of nitrification on denitrification as a ubiquitous and unifying feature of environmental nitrogen cycling. *Proc. Natl. Acad. Sci. U. S. A.* **113**, E6391–E6400 (2016).
30. K. L. Casciotti, Nitrogen and Oxygen Isotopic Studies of the Marine Nitrogen Cycle. *Ann. Rev. Mar. Sci.* **8**, 379–407 (2016).
31. J. Granger J and D.M. Sigman. Removal of nitrite with sulfamic acid for nitrate N and O isotope analysis with the denitrifier method. *Rapid Commun. Mass Spectrom.* **23**, 3753–3762 (2009).
32. L. A. Treibergs, J. Granger, Enzyme level N and O isotope effects of assimilatory and dissimilatory nitrate reduction. *Limnol. Oceanogr.* **62**, 272–288 (2017).
33. C. Buchwald, K. L. Casciotti, Oxygen isotopic fractionation and exchange during bacterial nitrite oxidation. *Limnol. Oceanogr.* **55**, 1064–1074 (2010).
34. T. C. Hollocher, Source of the oxygen atoms of nitrate in the oxidation of nitrite by

Nitrobacter agilis and evidence against a PON anhydride mechanism in oxidative phosphorylation. *Arch. Biochem. Biophys.* **233**, 721–727 (1984).

35. D. M. Sigman, *et al.*, Coupled nitrogen and oxygen isotope measurements of nitrate along the eastern North Pacific margin. *Global Biogeochem. Cycles* **19**, GB4022 (2005).

36. K. L. Casciotti, M. R. McIlvin, Isotopic analyses of nitrate and nitrite from reference mixtures and application to Eastern Tropical North Pacific waters. *Mar. Chem.* **107**, 184–201 (2007).

37. B. J. Callahan, *et al.*, DADA2: High-resolution sample inference from Illumina amplicon data. *Nat. Methods* **13**, 581–583 (2016).

38. J. J. Wright, K. M. Konwar, S. J. Hallam, Microbial ecology of expanding oxygen minimum zones. *Nat. Rev. Microbiol.* **10**, 381–394 (2012).

39. S. Lücker, B. Nowka, T. Rattei, E. Spieck, H. Daims, The genome of Nitrospina gracilis illuminates the metabolism and evolution of the major marine nitrite oxidizer. *Front. Microbiol.* **4**, 27 (2013).

40. H. Daims, S. Lücker, M. Wagner, A New Perspective on Microbes Formerly Known as Nitrite-Oxidizing Bacteria. *Trends Microbiol.* **24**, 699–712 (2016).

41. K. F. Ettwig, *et al.*, Nitrite-driven anaerobic methane oxidation by oxygenic bacteria. *Nature* **464**, 543–548 (2010).

42. B. Thamdrup, *et al.*, Anaerobic methane oxidation is an important sink for methane in the ocean's largest oxygen minimum zone. *Limnol. Oceanogr.* **64**, 2569–2585 (2019).

43. D. E. Canfield, *et al.*, A Cryptic Sulfur Cycle in Oxygen-Minimum-Zone Waters off the Chilean Coast. *Science* **330**, 1375–1378 (2010).

44. F. J. Pavia, *et al.*, Shallow particulate organic carbon regeneration in the South Pacific Ocean. *Proc. Natl. Acad. Sci. U. S. A.* **116**, 9753–9758 (2019).

45. D. A. Stolper, N. P. Revsbech, D. E. Canfield, Aerobic growth at nanomolar oxygen concentrations. *Proc. Natl. Acad. Sci. U. S. A.* **107**, 18755–18760 (2010).

46. R. L. Morris, T. M. Schmidt, Shallow breathing: Bacterial life at low O 2. *Nat. Rev. Microbiol.* **11**, 205–212 (2013).

47. E. J. Zakem, M. J. Follows, A theoretical basis for a nanomolar critical oxygen concentration. *Limnol. Oceanogr.* **62**, 795–805 (2017).

48. C. Deutsch, H. Brix, T. Ito, H. Frenzel, L. A. Thompson, Climate-forced variability of

ocean hypoxia. *Science* **333**, 336–339 (2011).

49. J.M. Beman, J.M. and M.T. Carolan, Deoxygenation alters bacterial diversity and community composition in the ocean's largest oxygen minimum zone. *Nature Comm.* **4**, 1-11 (2013).

50. J. M. Wilson, S. Y. Litvin, J. M. Beman, Microbial community networks associated with variations in community respiration rates during upwelling in nearshore Monterey Bay, California. *Environ. Microbiol. Rep.* **10**, 272–282 (2018).

51. K. L. Casciotti, D. M. Sigman, M. G. Hastings, J. K. Böhlke, A. Hilkert, Measurement of the oxygen isotopic composition of nitrate in seawater and freshwater using the denitrifier method. *Anal. Chem.* **74**, 4905–4912 (2002).

52. D. M. Sigman, *et al.*, A bacterial method for the nitrogen isotopic analysis of nitrate in seawater and freshwater. *Anal. Chem.* **73**, 4145–4153 (2001).

53. B. B. Ward, K. A. Kilpatrick, E. H. Renger, R. W. Eppley, Biological nitrogen cycling in the nitracline. *Limnol. Oceanogr.* **34**, 493–513 (1989).

54. C. Ritz, F. Baty, J. C. Streibig, D. Gerhard, Dose-response analysis using R. *PLoS One* **10** (2015).

Figures (for initial submission)

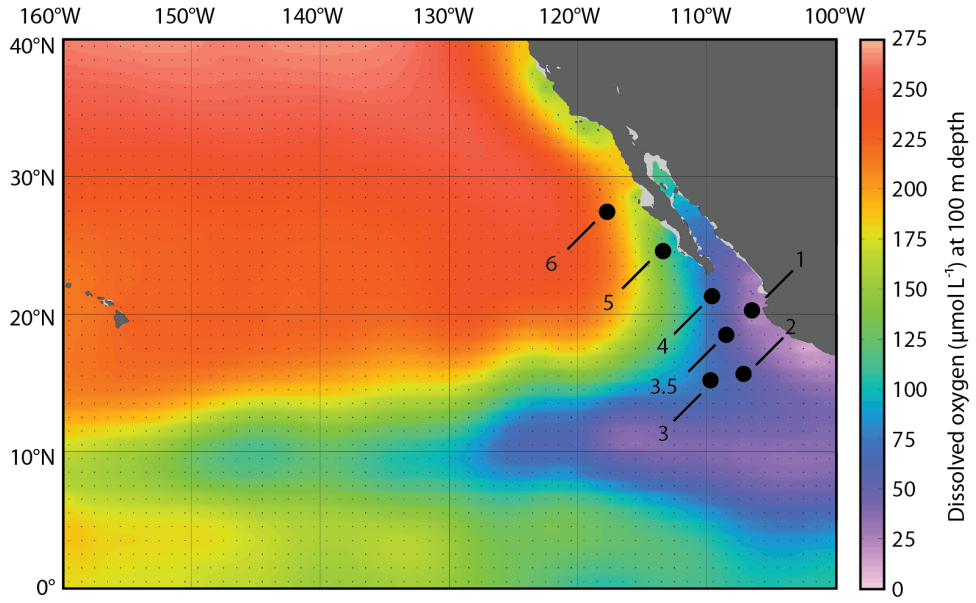

Figure 1: Station locations (numbered black circles) in the ETNP plotted on dissolved oxygen concentrations (in µM) at 100 m depth from the World Ocean Atlas.

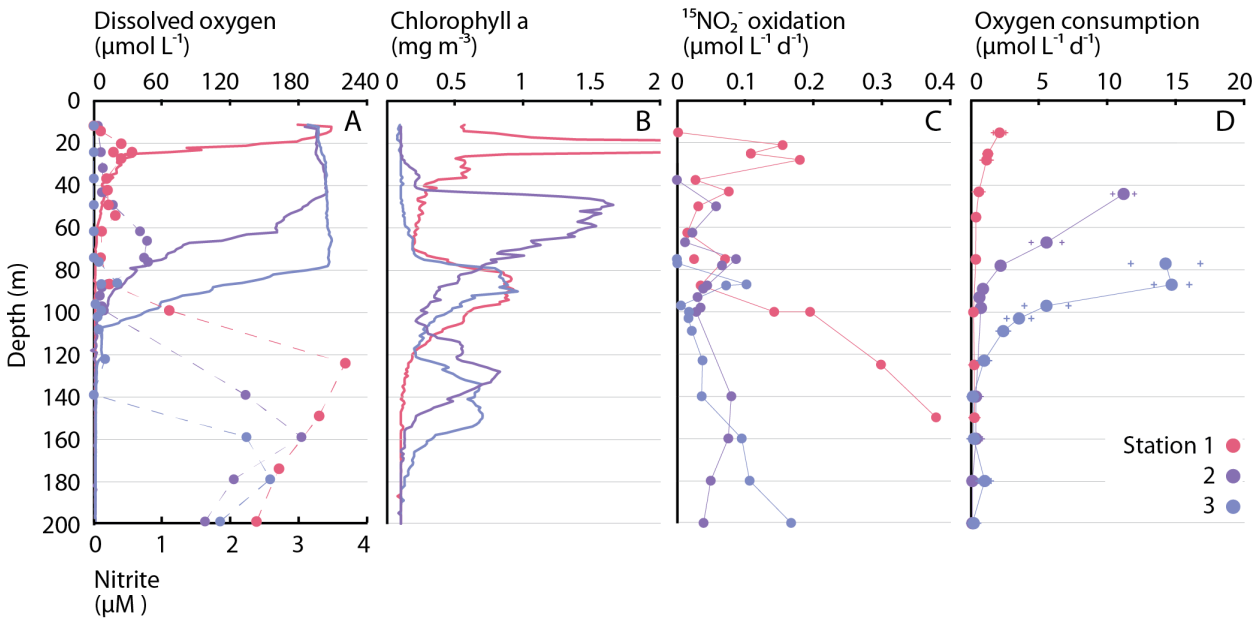

Figure 2: Depth profiles of (A) DO (solid lines) and nitrite (data points connected by dashed lines), (B) chlorophyll a, (C) nitrite oxidation rates, and (D) OCR (error bars denote standard deviation of five replicates) show consistent variation across Stations 1-3 (denoted by different colors). Maximum chlorophyll values at Station 1 plot off-axis.

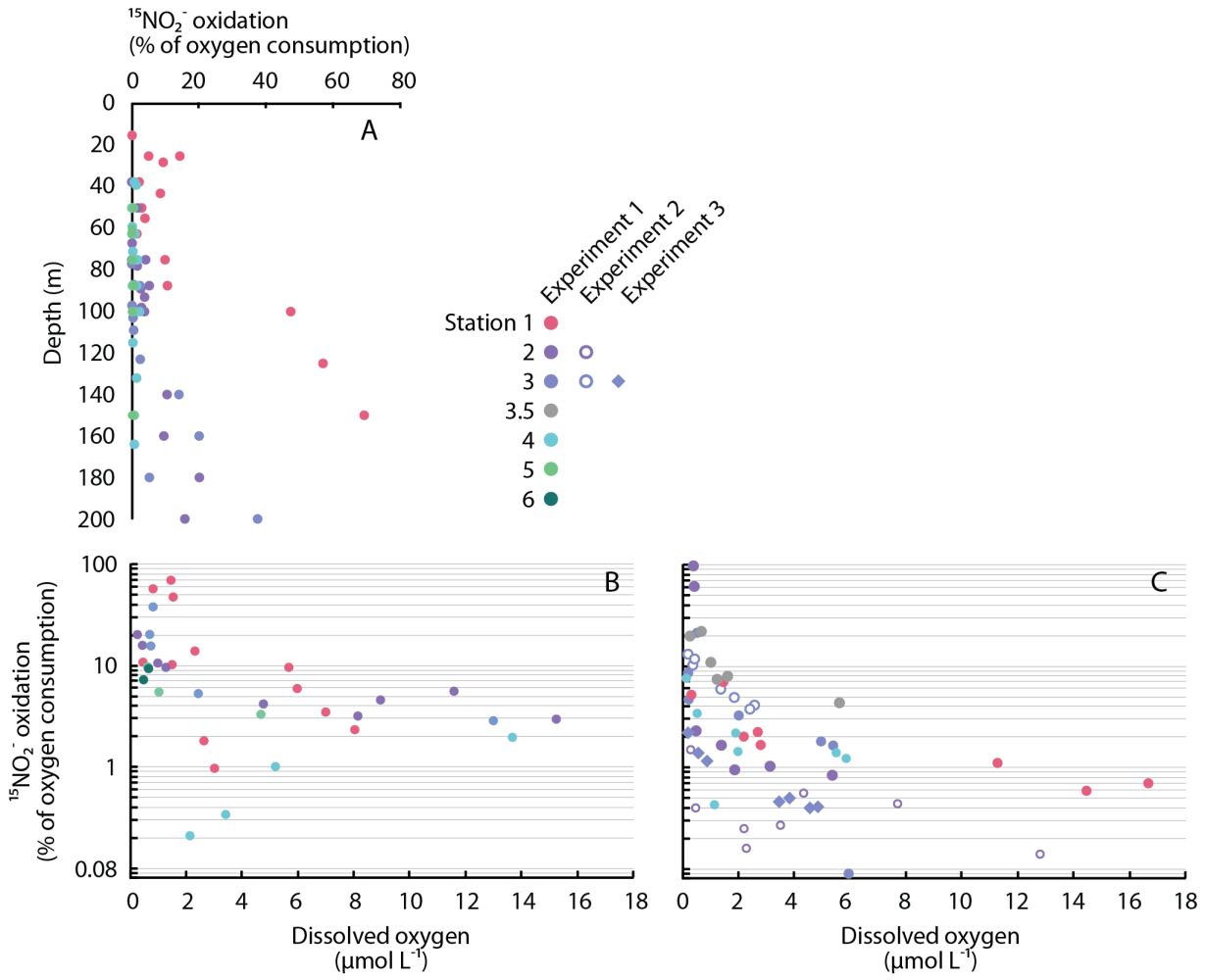

Figure 3: DO consumption via nitrite oxidation as a percentage of OCR with (A) depth, and as a function of DO in (B) depth profiles and (C) oxygen manipulation experiments. Colors denote different stations. Only measurements for DO <18 μM are included in panel B. All experimental bottles with dual nitrite oxidation and OCR are shown in C; and different symbols denote different experiments.

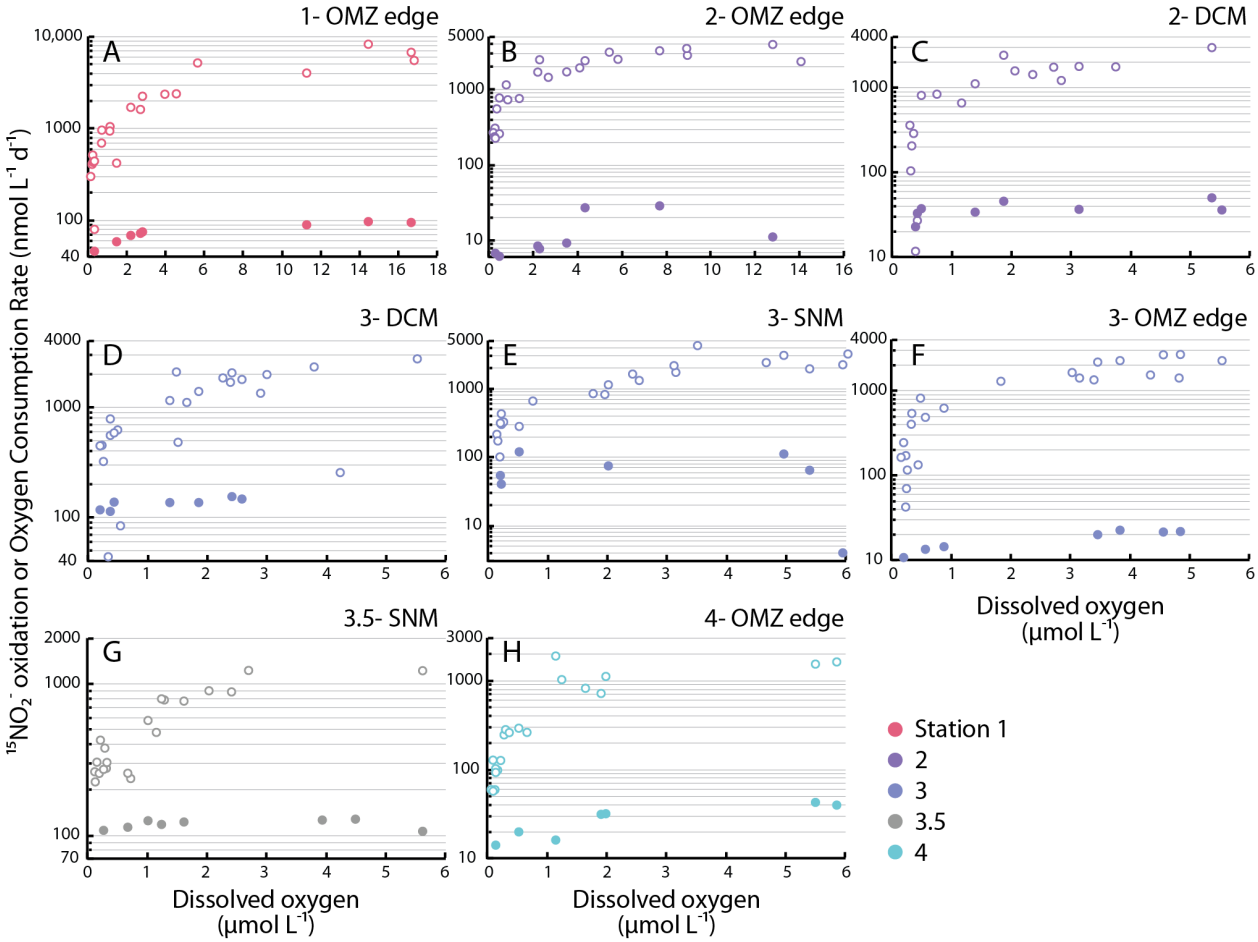

Figure 4: Nitrite oxidation rates (filled symbols) and OCR (open symbols) as a function of DO in oxygen manipulation experiments. Colors denote different stations, with panels displaying data from different experiments: A) Station 1 OMZ edge (20 µM DO), B) Station 2 OMZ edge, C) Station 2 DCM, D) Station 3 DCM, E) Station 3 SNM, F) Station 3 OMZ edge, G) Station 3.5 SNM, and H) Station 4 OMZ edge. Note differences in vertical axes between experiments, and differences in horizontal axes in panels A and B compared with the remaining panels.

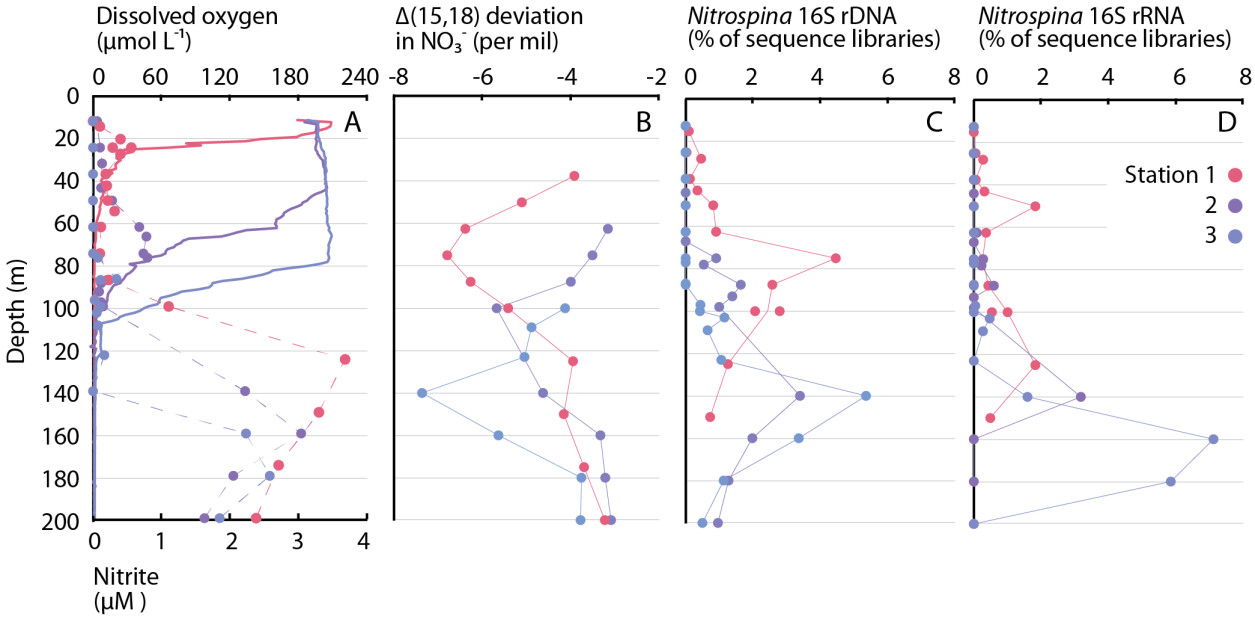

Figure 5: Depth profiles of (A) DO (solid lines) and nitrite (data points connected by dashed lines), (B) Δ(15,18) dual-isotope deviations in nitrate, and *Nitrospina* ASVs as a percentage of (C)16S rDNA sequence libraries and (D) 16S rRNA sequence libraries. Colors denote different sampling stations.

Table 1: Oxygen manipulation experiments and calculated parameters for OCR and nitrite oxidation rates

Sta.	Depth (m)	Type	OCR			Nitrite oxidation		
			v_{max} (nM d^{-1})	K_s (nM)	r^2	v_{max} (nM d^{-1})	K_s (nM)	r^2
1	46	OMZ edge	12005	13390	.892	94.5	611	.861
2	90	OMZ edge	4164	3262	.878	23.3	1876	.347
2	140	DCM	5426	5674	.811	43.9	185	.445
3	130	DCM	2765	18040	.569	149	63.8	.665
3	170	SNM	5973	6382	.757	71.2	38.4	.019
3	110	OMZ edge	4025	4247	.868	23.0	346	.910
3.5	80	SNM	1612	1621	.846	122	34.1	.269
4	100	OMZ edge	2075	1738	.776	47.5	1015	.825

636 **Table 2:** Relative abundance of *Nitrospina* reads, functional genes from *Nitrospina*, and
637 *Prochlorococcus* reads within metagenomes (expressed per million reads)
638

Sta.	Depth	Type	*Nitrospina*	Nitrite oxido-reductase	Cyto-chrome c	Cyto-chrome bd	Chlorite disumtase	*Prochloro-coccus*
1	25	OMZ edge	1084	2	0	0	1	865
1	87.5	DCM	31920	65	14	2	11	47992
1	100	SNM	21196	37	22	2	7	10765
2	89	OMZ edge	22442	38	12	10	14	57194
2	130	DCM	33290	57	20	4	11	33522
2	160	SNM	21725	37	18	2	4	4157
3	123	OMZ edge	18647	34	10	2	11	54709
3	140	DCM	34227	55	18	4	12	37202
3	180	SNM	17617	30	17	2	4	4881

639